

Spectral evidence for Dirac spinons in a kagome lattice antiferromagnet

Received: 20 October 2023

Accepted: 28 March 2024

Published online: 09 May 2024

 Check for updates

Zhenyuan Zeng^{1,2}, Chengkang Zhou³, Honglin Zhou^{1,2}, Lankun Han^{1,2}, Runze Chi^{1,2}, Kuo Li⁴, Maiko Kofu⁵, Kenji Nakajima⁵  , Yuan Wei⁶, Wenliang Zhang⁶, Daniel G. Mazzone⁷, Zi Yang Meng³   & Shiliang Li^{1,2,8}  

Emergent quasiparticles with a Dirac dispersion in condensed matter systems can be described by the Dirac equation for relativistic electrons, in analogy with Dirac particles in high-energy physics. For example, electrons with a Dirac dispersion have been intensively studied in electronic systems such as graphene and topological insulators. However, charge is not a prerequisite for Dirac fermions, and the emergence of Dirac fermions without a charge degree of freedom has been theoretically predicted to be realized in Dirac quantum spin liquids. These quasiparticles carry a spin of 1/2 but are charge-neutral and so are called spinons. Here we show that the spin excitations of a kagome antiferromagnet, $\text{YCu}_3(\text{OD})_6\text{Br}_2$ [$\text{Br}_{0.33}(\text{OD})_{0.67}$], are conical with a spin continuum inside, which is consistent with the convolution of two Dirac spinons. The predictions of a Dirac spin liquid model with a spinon velocity obtained from spectral measurements are in agreement with the low-temperature specific heat of the sample. Our results, thus, provide spectral evidence for a Dirac quantum spin liquid state emerging in this kagome lattice antiferromagnet. However, the locations of the conical spin excitations differ from those calculated by the nearest-neighbour Heisenberg model, suggesting the Dirac spinons have an unexpected origin.

Quantum spin liquids (QSLs) are an ideal platform for realizing quantum states of matter beyond the Landau paradigm of symmetry and its spontaneous breaking^{1–4}. One of the crucial features of QSLs is the presence of fractionalized excitations, which have the form of elemental quasiparticles carrying the topological nature and interacting with the emergent gauge field^{5–10}. Spinons are fractionalized excitations in the sense that they carry a spin of 1/2 but are charge-neutral. The spinons can be gapped or gapless. In the gapless state, the spinons can have a conical shape dispersion with the apex at zero energy. Their spectrum

is like that of the Dirac cones in the electronic band structures of graphene and topological insulators^{11–13}. Therefore, the spinons in Dirac QSLs are a new kind of Dirac quasiparticle without the charge degree of freedom. Although a Dirac QSL is interesting in its own right, it also serves as the parent state of novel two-dimensional quantum phases characterized by emergence and deconfinement^{14–17}. Although Dirac QSLs have been highly anticipated in many theoretical models of different kinds of lattices^{18–32}, their material realization has remained elusive due to the lack of spectral evidence.

¹Beijing National Laboratory for Condensed Matter Physics, Institute of Physics, Chinese Academy of Sciences, Beijing, China. ²School of Physical Sciences, University of Chinese Academy of Sciences, Beijing, China. ³Department of Physics and HKU-UCAS Joint Institute of Theoretical and Computational Physics, The University of Hong Kong, Hong Kong SAR, China. ⁴Center for High Pressure Science and Technology Advanced Research, Beijing, China. ⁵J-PARC Center, Japan Atomic Energy Agency, Tokai, Japan. ⁶Photon Science Division, Paul Scherrer Institut, Villigen, Switzerland. ⁷Laboratory for Neutron Scattering and Imaging, Paul Scherrer Institut, Villigen, Switzerland. ⁸Songshan Lake Materials Laboratory, Dongguan, China.  e-mail: kenji.nakajima@j-parc.jp; zymeng@hku.hk; slli@iphy.ac.cn

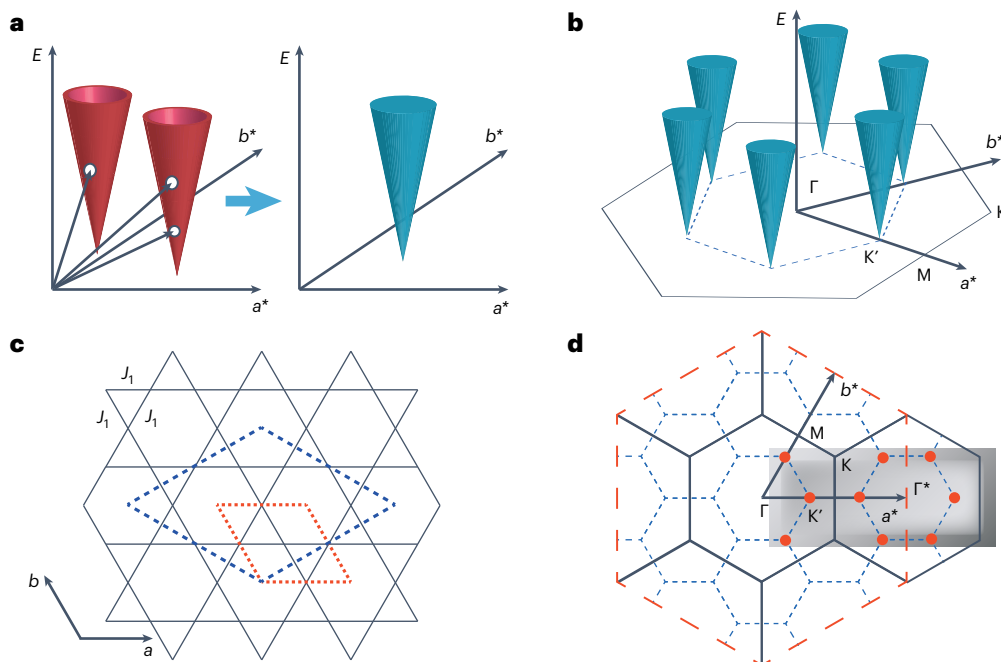


Fig. 1 | Schematics of low-energy conical spin excitations and reciprocal space for $\text{YCu}_3\text{-Br}$. **a**, Schematic illustration of two Dirac spinons with a conical-surface dispersion (red) that merge into a cone spin excitation with a continuum inside (blue). The two spinons can come from either two different Dirac cones or the same one, as indicated by the white dots. a^* and b^* are the lattice parameters in the reciprocal lattice. **b**, Six conical low-energy spin excitations in $\text{YCu}_3\text{-Br}$. Their momenta in the kagome Brillouin zone is indicated. **c**, The in-plane kagome

structure. The dashed red and blue lines represent the lattice unit cells of $\text{YCu}_3\text{-Br}$ and $\text{Y}_3\text{Cu}_9(\text{OH})_{19}\text{Cl}_8$ (ref. 42), respectively. **d**, Sketch of the in-plane reciprocal space. The black solid line and the red and blue dashed lines represent the kagome, the extended kagome and the lattice of the $\text{Y}_3\text{Cu}_9(\text{OH})_{19}\text{Cl}_8$ Brillouin zones, respectively. The grey shaded area illustrates the regime measured in this work.

Although it is hard to directly detect single spinon excitations, two spin excitations with total spin quantum number $S = 1$ can result in a spin continuum that can be revealed by inelastic neutron scattering (INS). For Dirac spinons, one would expect that the spin excitations exhibit a convolved cone structure with a finite and continuous spectral weight inside the cone (unlike the spin wave of linear dispersing magnons that have no weight inside the cone) and with an apex at zero energy with respect to the ground state of the spin system^{31,32}, as illustrated in Fig. 1a. In materials that have been theoretically suggested to host Dirac QSLs (refs. 20, 27, 29), the spin excitations observed in INS experiments either do not look like Dirac spinons or are too blurry for their nature to be determined^{33–36}.

The discovery in this work changes the situation. The material studied in this work is $\text{YCu}_3(\text{OH})_6\text{Br}_2[\text{Br}_{1-x}(\text{OH})_x]$ (denoted as $\text{YCu}_3\text{-Br}$ hereafter). It has perfect kagome planes formed by Cu^{2+} ions with $S = 1/2$ (ref. 37). Previous measurements have shown that there is no magnetic ordering down to 50 mK although its Weiss temperature is about -80 K (refs. 38–41). Moreover, the low-temperature specific heat shows a T^2 dependence at zero field and a T -linear term under a field³⁸, which is consistent with a Dirac QSL (ref. 20). Indeed, our neutron scattering results presented in this work for $\text{YCu}_3\text{-Br}$ ($x = 0.67$) clearly reveal six conical spin excitations with filled continuum weights inside the cones (Fig. 1b,d). This represents strong evidence that the material realizes the long-sought-after Dirac QSL.

Figure 2a–d shows contour plots of the in-plane low-energy excitations at several energies at 0.3 K for the deuterated $\text{YCu}_3\text{-Br}$. Six symmetrical spin excitations are centred at $(1, 0)$ in the second Brillouin zone. The positions are at $(2/3, 0)$ and the corresponding sixfold rotational points about the c^* axis at $(1, 0)$. Note that these positions correspond to the K' points in Fig. 1d. The peaks at 0.2 meV in Fig. 2a are sharp and elongated along the direction vertical to Q due to sample mosaic. With increasing energy (Fig. 2b–d), the peaks become broader,

but no ring-like structure is observed at any energy and the excitations are always continuum with filled cones. Figure 2e shows an E - Q plot with Q along the $[H, 0]$ direction. One can clearly see two filled cone-like excitations at $(2/3, 0)$ and $(4/3, 0)$, which disappear at 30 K (Fig. 2f), confirming the magnetic origin of these excitations.

To further quantitatively analyse the data, we made a cut along the $[H, 0]$ direction at 0.2 meV, as shown in Fig. 3a. Besides the peaks at $(2/3, 0)$ and $(4/3, 0)$, there is also a peak at $(1/3, 0)$. This suggests that the spin excitations also existed in the first Brillouin zone of the kagome lattice. Figure 3b shows the integrated intensity of the peaks normalized by the magnetic form factor as a function of the in-plane $|Q_{\text{in}}| = |[H, K]|$. The integrated intensity is fitted well by $A(1 - \cos(\pi|Q_{\text{in}}|/|Q_{(1,0)}|))$, where A is the only fitting parameter. This function explains why the intensity of the $(1/3, 0)$ peak is much weaker and resembles the structure factor of randomly arranged nearest-neighbour singlets³³. In a similar system with long-range antiferromagnetic order⁴², the spin excitations were also very strong in the second kagome Brillouin zone. Whether the fitting observed in Fig. 3b is coincidental or has a deeper physical meaning warrants further theoretical investigation. It is important to emphasize that the spin excitations around the peak positions do not follow the structure factor of randomly arranged nearest-neighbour singlets but exhibit Lorentzian behaviour, as described below. Figure 3c shows the Q cuts along the $[H, 0]$ direction at $(2/3, 0)$, which can all be well fitted by the Lorentzian function. The fitted full-width at half-maximum (FWHM) at 0.12 meV is about $0.035 \pm 0.007 \text{ \AA}^{-1}$, which corresponds to a spin-spin correlation of about 180 \AA without considering the instrumental resolution. Moreover, the FWHM shows a linear dependence below 0.6 meV (Fig. 3d), which has a slope and intercept of $0.147 \text{ \AA}^{-1} \text{ meV}^{-1}$ and 0.016 \AA^{-1} , respectively. Note that the latter is very close to the instrumental resolution (Supplementary Information). The slope provides information about the velocity of spinons v_F if the cone spin excitations come from the convolution of two Dirac spinons. The value is about

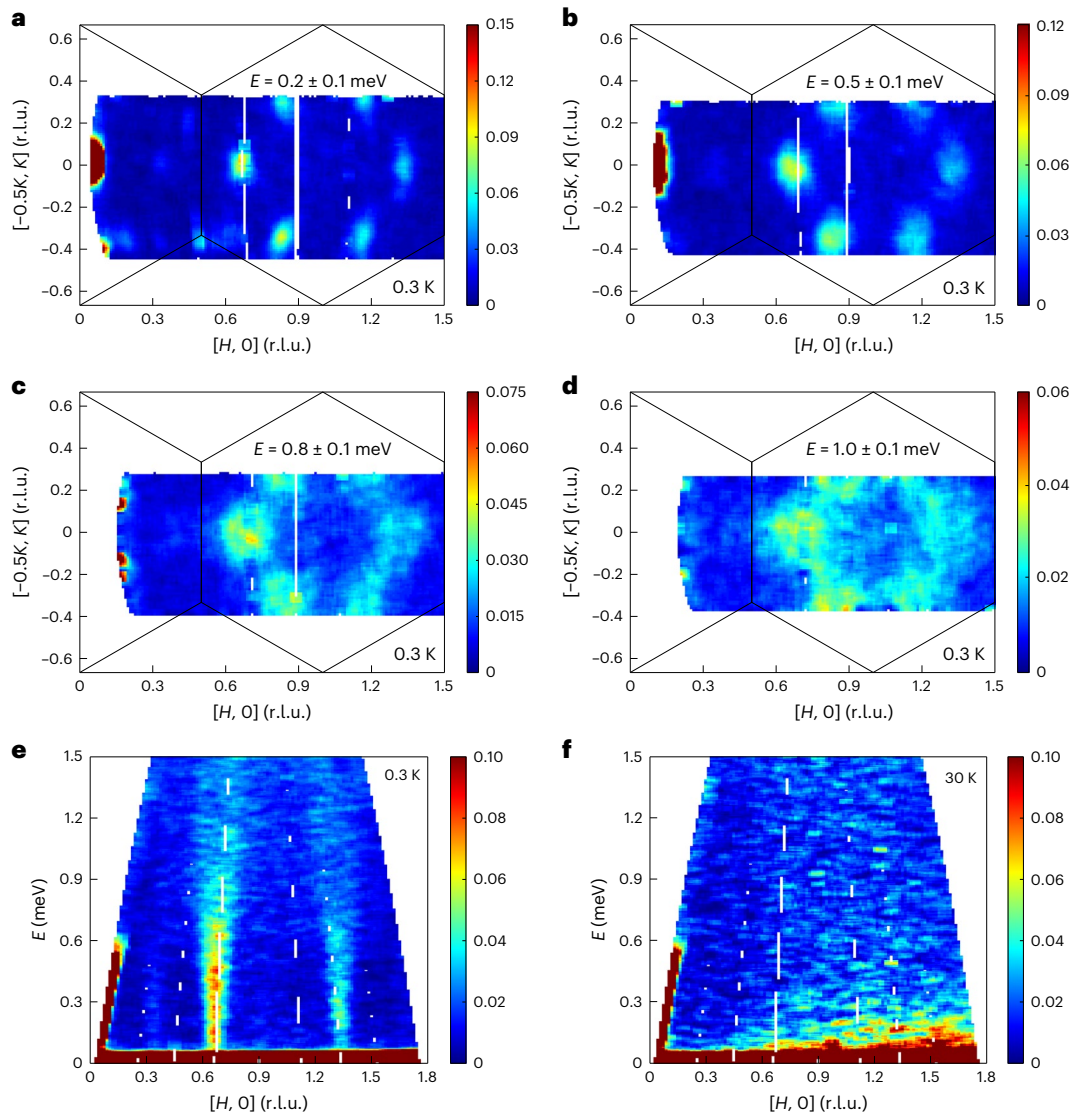


Fig. 2 | INS results at low energies with the incident energy of neutrons (E_i) = 2.566 meV. a–d, Intensity contour plots of the INS results at 0.3 K in the $[H, K]$ zone at 0.2 meV (a), 0.5 meV (b), 0.8 meV (c) and 1 meV (d). The \pm symbol gives the integrated energy range. The solid lines forming the hexagons mark the kagome Brillouin zones. The x and y axes are the components of Q parallel to $(H, 0)$ and

$(-0.5K, K)$, respectively. The positions of the excitations are at $(1 \pm 1/3, 0)$, $(1, \pm 1/3)$ and $(1 \pm 1/3, \mp 1/3)$. **e, f**, Intensity contour plots of the INS results as a function of E and Q along the $[H, 0]$ direction at 0.3 K (e) and 30 K (f). The integrated range along $[-K/2, K/2]$ is from $K = -0.05$ to 0.05 . r.l.u. is the reciprocal lattice unit.

$1 \times 10^3 \text{ m s}^{-1}$ for free spinons, and there could be renormalization due to interaction effects and the detailed fusion behaviour of two spinons.

The high-energy spin excitations of $\text{YCu}_3\text{-Br}$ are shown in Fig. 4. At 1.3 meV, the excitations become so broad that they seem to be connected with those in adjacent zones (Fig. 4a). With increasing energy, the jointed six-branch spin excitations merge into one centred around $(1, 0)$, and the area becomes smaller with increasing energy, as shown in Fig. 4b–d. The top of the excitations ends at about 7.5 meV (Fig. 4e), which is about 100 times the lowest energy observed. Unlike the low-energy spin excitations, the high-energy spin excitations survive at 30 K although there is substantial broadening (Fig. 4f).

As we can observe the whole spectra within the second kagome Brillouin zone, the static susceptibility $\chi'(Q, 0)$ can be obtained from the imaginary part of the dynamical susceptibility $\chi''(Q, \omega)$ by the Kramers–Kronig relation,

$$\chi'(Q, 0) \propto \int_{-\infty}^{\infty} \frac{\chi''(Q, \omega)}{\omega} d\omega. \quad (1)$$

According to the fluctuation-dissipation theorem, we have $\chi''(Q, \omega) = S(Q, \omega)[1 - \exp(-\hbar\omega/k_B T)]$, where $S(Q, \omega)$ is the scattering function that is proportional to the signal obtained from the INS measurements, \hbar is the Planck's constant divided by 2π and k_B is the Boltzmann constant. Moreover, as $\chi''(Q, \omega)$ is the odd function of the energy, the integration can be done by just considering $S(Q, \omega)$ at positive energy. The calculated result is shown in Fig. 4g, where there are still six symmetrical peaks. Figure 4h shows the H cut at the $(4/3, 0)$ peak and its Lorentzian fit. The magnetic correlation length ξ is, thus, calculated to be about 83 Å without considering the instrumental resolution, which is about 25 Cu–Cu bond lengths.

Our results provide strong evidence for an emerging Dirac QSL state in $\text{YCu}_3\text{-Br}$. The key finding in our work is the low-energy conical spin excitations with a continuum inside, which requires a non-trivial origin of the low-energy excitations. For the conical spin excitations, trivial explanations such as damped spin waves in the presence of strong disorder cannot simultaneously reproduce the sharp excitations near zero energy and the broad spectra at higher

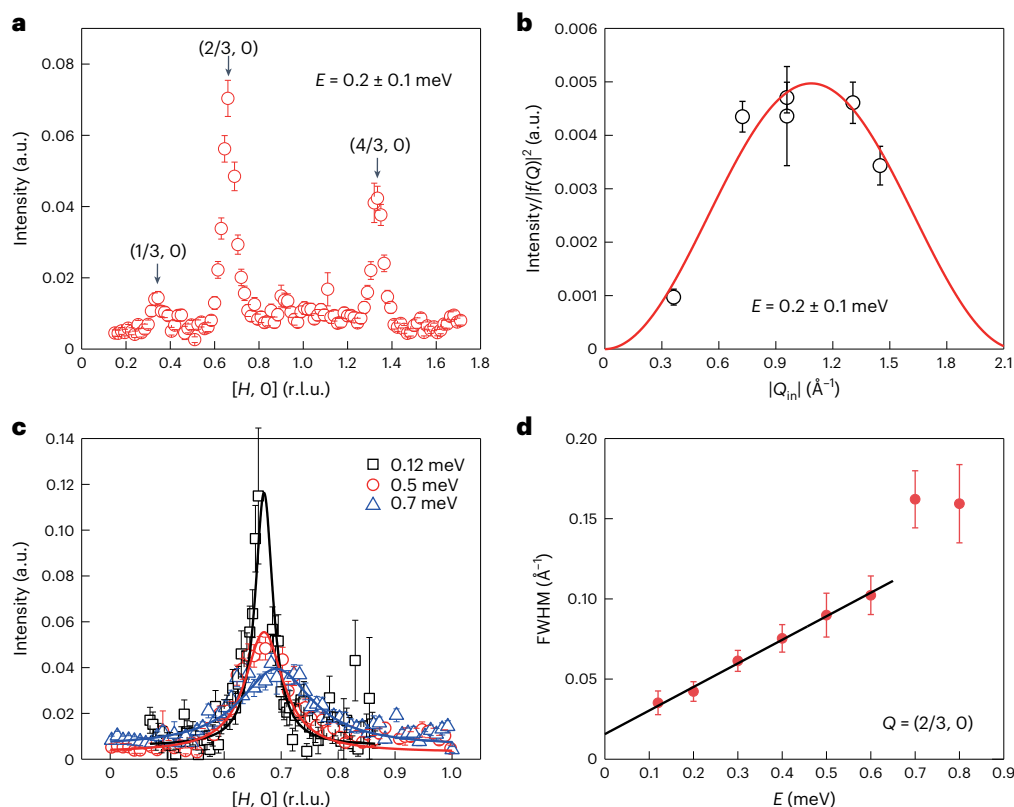


Fig. 3 | Quantitative analysis of the low-energy data at 0.3 K. **a**, Constant E cuts along the $[H, 0]$ direction at 0.2 meV. **b**, The in-plane $|Q_{in}|$ dependence of the integrated intensity of the peaks at 0.2 meV, which has been normalized to the square of the magnetic form factor of the Cu^{2+} ion. The solid line is the fit to a cosine function, as described. **c**, Constant E cuts along the $[H, 0]$ direction at

several energies near $(2/3, 0)$. The solid lines are fits to the Lorentzian function. **d**, The energy dependence of the FWHM at $Q = (2/3, 0)$. The solid line is a linear fit. The error bars in all panels represent one-standard-deviation uncertainty in the data based on Poisson statistics with the sample size being the neutron counts. arb. unit, arbitrary unit.

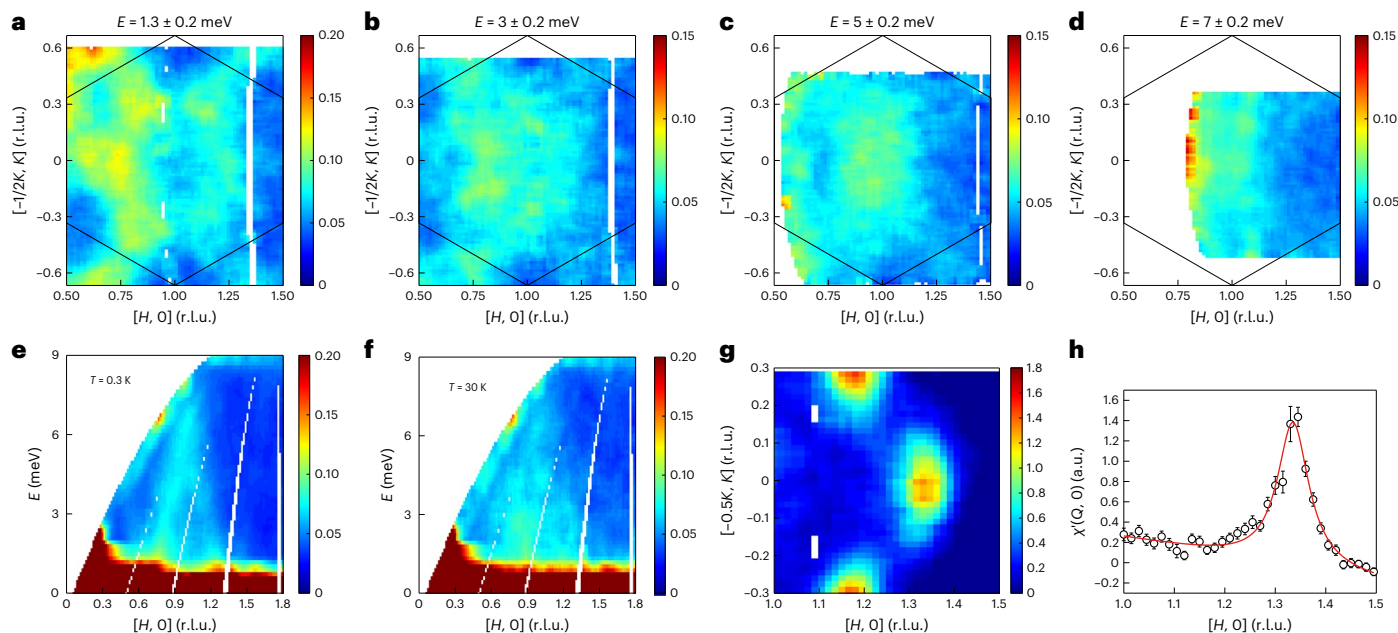


Fig. 4 | High-energy spin excitations at $E_s = 9.986$ meV and static susceptibility $\chi'(Q, 0)$ in YCu_3Br . **a–d**, Intensity contour plots of the INS results at 0.3 K in the $[H, K]$ zone at 1.3 meV (**a**), 3 meV (**b**), 5 meV (**c**) and 7 meV (**d**). **e, f**, Intensity contour plots of the INS results as a function of E and Q along the $[H, 0]$ direction at 0.3 K (**e**) and 30 K (**f**). Note that the intensities at small Q near the edge of the colour map (**c–f**) are from the background. **g**, $\chi'(Q, 0)$ at 0.3 K

calculated by the Kramers–Kronig relation based on $S(Q, \omega)$ between 0.075 and 8 meV. Only half of the Brillouin zone is shown to avoid the background at lower Q 's. **h**, H dependence of $\chi'(Q, 0)$ around $(4/3, 0)$. The solid line is the fit to the Lorentzian function with a linear background. The error bars represent the one-standard-deviation uncertainty in the data based on Poisson statistics with the sample size being the neutron counts.

energies (Supplementary Information). The low-energy spinon continuum due to strong disorder always extends to a large area in the momentum space at low energies as disorder tends to destroy the spin–spin correlation and always reduces the spin–spin correlation length^{43–47}. In contrast, these features can be explained well by the presence of Dirac spinons, which result in conical spin excitations by two-spinon convolution²⁰. The picture based on Dirac spinons also gives us a quantitative comparison between the INS and specific-heat measurements. According to a previous report³⁸, the low-temperature specific heat of YCu₃-Br exhibited a quadratic temperature dependence at zero field, that is, $C = \alpha T^2$. Theoretically, α can be calculated as $\alpha = 0.586 \text{ J mol}^{-1} \text{ K}^{-3}$ (ref. 20), where we have used that $v_F \approx 10^3 \text{ m s}^{-1}$ and there are six Dirac fermions. This is indeed very close to the experimental value, $0.452 \text{ J mol}^{-1} \text{ K}^{-3}$. Note that thermal-conductivity (κ) measurements of YCu₃-Br failed to detect a non-zero $\kappa/T|_{T \rightarrow 0\text{K}}$ under a field⁴¹, which does not seem to agree with the existence of spinon Fermi surfaces induced by a field. However, as $\kappa = (1/3)Cv_F l$, a very large mean free path ($l > 30 \mu\text{m}$) is required for the spinons to be detected by heat-transport measurements ($\kappa/T > 0.01 \text{ mW K}^{-2} \text{ cm}^{-1}$). Such a large value of l is apparently hard to achieve considering the site disorder in this system^{37–39}. Also note that our results clearly show excitations down to 0.06 meV, which is much smaller than the gap value determined by the heat-transport measurement⁴¹, suggesting that the system has a gapless ground state.

The Dirac QSL state in YCu₃-Br is not the one predicted by the nearest Heisenberg model, which should exhibit conical spin excitations at (0.5, 0) (the point M in Fig. 1d)²⁶. The position of the spin excitations indicates that the magnetic system may be related to the $Q = (1/3, 1/3)$ phase⁴⁸, which suggests that there are three different nearest exchanges J_1 (Fig. 1c). Although this order seems closely related to Y₃Cu₉(OH)₉Cl₈ (ref. 42), which has distorted kagome planes and an enlarged lattice unit cell as shown in Fig. 1c, the kagome lattice remains undistorted in our sample. What is surprising is that the spin excitations close to zero energy are very sharp in our sample, and actually, much sharper than those in the ordered sample⁴², which seems to suggest that the emergent Dirac spinons are insensitive to disorder. A detailed discussion of the spectrum of spin waves calculated in the presence of disorder in the form of different J_1 and the contrast with respect to our INS results are given in the Supplementary Information. Whether the melting of the above order can result in a Dirac QSL is an open question. Note that an 1/9 magnetization plateau and magnetic quantum oscillations have been observed in this system⁴⁹, which were explained by a model assuming that a Dirac spinon was coupled with the emergent gauge field, consistent with our observation of conical spin excitations.

Finding a QSL state in the YCu₃-Br system seemingly with disorder is surprising, as it is believed that disorder will typically destroy QSLs (ref. 50). In our case, the disorder is mainly site disorder of Y³⁺, Br[−] and (OH)[−], which results in alternate bonds of the hexagons in the kagome³⁹. Note that the undistorted hexagons may also be treated as disorder to the hexagons with alternate bonds, which are related to the $Q = (1/3, 1/3)$ phase⁴⁸, depending on which quantity of hexagons is larger. Our results show that disorder has a negligible effect on the low-energy spin excitations. This is consistent with the observation of magnetic quantum oscillations in this system⁴⁹, which typically requires a clean system. This means that the Dirac QSL is either robust against disorder^{51,52} or even induced by disorder^{53,54}. At this stage, an unambiguous theoretical calculation with disorder and longer-range interactions of the dynamic spectrum of frustrated quantum spin models is difficult and subject to approximations such as finite size, finite temperature, finite bond-dimension and so on⁵⁵. On the other hand, the conic spin excitations emerging from Dirac spinons will render the very low-energy spin excitations with a sharp energy–momentum boundary^{14,15,30,31}, as observed here. Overall, the YCu₃-Br system is an interesting platform for further experimental and theoretical studies.

Online content

Any methods, additional references, Nature Portfolio reporting summaries, source data, extended data, supplementary information, acknowledgements, peer review information; details of author contributions and competing interests; and statements of data and code availability are available at <https://doi.org/10.1038/s41567-024-02495-z>.

References

- Balents, L. Spin liquids in frustrated magnets. *Nature* **464**, 199 (2010).
- Savary, L. & Balents, L. Quantum spin liquids: a review. *Rep. Prog. Phys.* **80**, 016502 (2017).
- Zhou, Y., Kanoda, K. & Ng, T.-K. Quantum spin liquid states. *Rev. Mod. Phys.* **89**, 025003 (2017).
- Broholm, C. et al. Quantum spin liquids. *Science* **367**, 263 (2020).
- Kivelson, S. A., Rokhsar, D. S. & Sethna, J. P. Topology of the resonating valence-bond state: solitons and high- T_c superconductivity. *Phys. Rev. B* **35**, 8865–8868 (1987).
- Wen, X. G. Mean-field theory of spin-liquid states with finite energy gap and topological orders. *Phys. Rev. B* **44**, 2664–2672 (1991).
- Wen, X.-G. Colloquium: zoo of quantum-topological phases of matter. *Rev. Mod. Phys.* **89**, 041004 (2017).
- Sun, G.-Y. et al. Dynamical signature of symmetry fractionalization in frustrated magnets. *Phys. Rev. Lett.* **121**, 077201 (2018).
- Wang, Y.-C., Cheng, M., Witczak-Krempa, W. & Meng, Z. Y. Fractionalized conductivity and emergent self-duality near topological phase transitions. *Nat. Commun.* **12**, 5347 (2021).
- Chatterjee, A., Ji, W. & Wen, X.-G. Emergent generalized symmetry and maximal symmetry-topological-order. Preprint at <https://arxiv.org/abs/2212.14432> (2022).
- Geim, A. K. & Novoselov, K. S. The rise of graphene. *Nat. Mater.* **6**, 183 (2007).
- Hasan, M. Z. & Kane, C. L. Colloquium: topological insulators. *Rev. Mod. Phys.* **82**, 3045–3067 (2010).
- Vafeek, O. & Vishwanath, A. Dirac fermions in solids: from high- T_c cuprates and graphene to topological insulators and Weyl semimetals. *Annu. Rev. Condens. Matter Phys.* **5**, 83 (2014).
- Qin, Y. Q. et al. Duality between the deconfined quantum-critical point and the bosonic topological transition. *Phys. Rev. X* **7**, 031052 (2017).
- Ma, N. et al. Dynamical signature of fractionalization at a deconfined quantum critical point. *Phys. Rev. B* **98**, 174421 (2018).
- Xu, X. Y. et al. Monte Carlo study of lattice compact quantum electrodynamics with fermionic matter: the parent state of quantum phases. *Phys. Rev. X* **9**, 021022 (2019).
- Song, X.-Y., Wang, C., Vishwanath, A. & He, Y.-C. Unifying description of competing orders in two-dimensional quantum magnets. *Nat. Commun.* **10**, 4254 (2019).
- Sachdev, S. Kagomé and triangular-lattice Heisenberg antiferromagnets: ordering from quantum fluctuations and quantum-disordered ground states with unconfined bosonic spinons. *Phys. Rev. B* **45**, 12377–12396 (1992).
- Hastings, M. B. Dirac structure, RVB, and Goldstone modes in the kagomé antiferromagnet. *Phys. Rev. B* **63**, 014413 (2000).
- Ran, Y., Hermele, M., Lee, P. A. & Wen, X.-G. Projected-wave-function study of the spin-1/2 Heisenberg model on the kagomé lattice. *Phys. Rev. Lett.* **98**, 117205 (2007).
- Hermele, M., Ran, Y., Lee, P. A. & Wen, X.-G. Properties of an algebraic spin liquid on the kagome lattice. *Phys. Rev. B* **77**, 224413 (2008).
- Iqbal, Y., Becca, F. & Poilblanc, D. Projected wave function study of \mathbb{Z}_2 spin liquids on the kagome lattice for the spin- \mathbb{Z}_2 quantum Heisenberg antiferromagnet. *Phys. Rev. B* **84**, 020407 (2011).

23. Iqbal, Y., Poilblanc, D. & Becca, F. Vanishing spin gap in a competing spin-liquid phase in the kagome Heisenberg antiferromagnet. *Phys. Rev. B* **89**, 020407 (2014).
24. He, Y.-C., Zaletel, M. P., Oshikawa, M. & Pollmann, F. Signatures of Dirac cones in a DMRG study of the kagome Heisenberg model. *Phys. Rev. X* **7**, 031020 (2017).
25. Liao, H. J. et al. Gapless spin-liquid ground state in the $s=1/2$ kagome antiferromagnet. *Phys. Rev. Lett.* **118**, 137202 (2017).
26. Zhu, W., Gong, S. & Sheng, D. N. Identifying spinon excitations from dynamic structure factor of spin-1/2 Heisenberg antiferromagnet on the kagome lattice. *Proc. Natl Acad. Sci. USA* **116**, 5437 (2019).
27. Zhu, Z., Maksimov, P. A., White, S. R. & Chernyshev, A. L. Topography of spin liquids on a triangular lattice. *Phys. Rev. Lett.* **120**, 207203 (2018).
28. Liu, Z.-X. & Normand, B. Dirac and chiral quantum spin liquids on the honeycomb lattice in a magnetic field. *Phys. Rev. Lett.* **120**, 187201 (2018).
29. Hu, S., Zhu, W., Eggert, S. & He, Y.-C. Dirac spin liquid on the spin-1/2 triangular Heisenberg antiferromagnet. *Phys. Rev. Lett.* **123**, 207203 (2019).
30. Song, X.-Y., He, Y.-C., Vishwanath, A. & Wang, C. From spinon band topology to the symmetry quantum numbers of monopoles in Dirac spin liquids. *Phys. Rev. X* **10**, 011033 (2020).
31. Nomura, Y. & Imada, M. Dirac-type nodal spin liquid revealed by refined quantum many-body solver using neural-network wave function, correlation ratio, and level spectroscopy. *Phys. Rev. X* **11**, 031034 (2021).
32. Da Liao, Y., Xu, X. Y., Meng, Z. Y. & Qi, Y. Dirac fermions with plaquette interactions. II. SU(4) phase diagram with Gross-Neveu criticality and quantum spin liquid. *Phys. Rev. B* **106**, 115149 (2022).
33. Han, T. H. et al. Fractionalized excitations in the spin-liquid state of a kagome-lattice antiferromagnet. *Nature* **492**, 406–410 (2012).
34. Shen, Y. et al. Evidence for a spinon Fermi surface in a triangular-lattice quantum-spin-liquid candidate. *Nature* **540**, 559 (2016).
35. Ding, L. et al. Gapless spin-liquid state in the structurally disorder-free triangular antiferromagnet NaYbO₂. *Phys. Rev. B* **100**, 144432 (2019).
36. Bordelon, M. M. et al. Spin excitations in the frustrated triangular lattice antiferromagnet NaYbO₂. *Phys. Rev. B* **101**, 224427 (2020).
37. Chen, X.-H., Huang, Y.-X., Pan, Y. & Mi, J.-X. Quantum spin liquid candidate YCu₃(OH)₆Br₂[Br_x(OH)_{1-x}] ($x \approx 0.51$): with an almost perfect kagomé layer. *J. Magn. Mater.* **512**, 167066 (2020).
38. Zeng, Z. et al. Possible Dirac quantum spin liquid in the kagome quantum antiferromagnet YCu₃(OH)₆Br₂[Br_x(OH)_{1-x}]. *Phys. Rev. B* **105**, L121109 (2022).
39. Liu, J. et al. Gapless spin liquid behavior in a kagome Heisenberg antiferromagnet with randomly distributed hexagons of alternate bonds. *Phys. Rev. B* **105**, 024418 (2022).
40. Lu, F. et al. The observation of quantum fluctuations in a kagome Heisenberg antiferromagnet. *Commun. Phys.* **5**, 272 (2022).
41. Hong, X. et al. Heat transport of the kagome Heisenberg quantum spin liquid candidate YCu₃(OH)_{6.5}Br_{2.5}: localized magnetic excitations and a putative spin gap. *Phys. Rev. B* **106**, L220406 (2022).
42. Chatterjee, D. et al. From spin liquid to magnetic ordering in the anisotropic kagome Y-kapellasite Y₃Cu₃(OH)₁₉Cl₈: a single-crystal study. *Phys. Rev. B* **107**, 125156 (2023).
43. Zhu, Z., Maksimov, P. A., White, S. R. & Chernyshev, A. L. Disorder-induced mimicry of a spin liquid in YbMgGaO₄. *Phys. Rev. Lett.* **119**, 157201 (2017).
44. Kimchi, I., Nahum, A. & Senthil, T. Valence bonds in random quantum magnets: theory and application to YbMgGaO₄. *Phys. Rev. X* **8**, 031028 (2018).
45. Ma, Z. et al. Disorder-induced broadening of the spin waves in the triangular-lattice quantum spin liquid candidate YbZnGaO₄. *Phys. Rev. B* **104**, 224433 (2021).
46. Shimokawa, T., Watanabe, K. & Kawamura, H. Static and dynamical spin correlations of the $S = \frac{1}{2}$ random-bond antiferromagnetic Heisenberg model on the triangular and kagome lattices. *Phys. Rev. B* **92**, 134407 (2015).
47. Han, T.-H. et al. Correlated impurities and intrinsic spin-liquid physics in the kagome material herbertsmithite. *Phys. Rev. B* **94**, 060409 (2016).
48. Hering, M. et al. Phase diagram of a distorted kagome antiferromagnet and application to Y-kapellasite. *npj Comput. Mater.* **8**, 10 (2022).
49. Zheng, G. et al. Unconventional magnetic oscillations in kagome Mott insulators. Preprint at arxiv.org/abs/2310.07989 (2023).
50. Dey, S. Destabilization of U(1) Dirac spin liquids on two-dimensional nonbipartite lattices by quenched disorder. *Phys. Rev. B* **102**, 235165 (2020).
51. Yang, K., Varjas, D., Bergholtz, E. J., Morampudi, S. & Wilczek, F. Exceptional dynamics of interacting spin liquids. *Phys. Rev. Res.* **4**, L042025 (2022).
52. Seifert, U. F. P., Willsher, J., Drescher, M., Pollmann, F. & Knolle, J. Spin-Peierls instability of the U(1) Dirac spin liquid. Preprint at arxiv.org/abs/2307.12295 (2023).
53. Savary, L. & Balents, L. Disorder-induced quantum spin liquid in spin ice pyrochlores. *Phys. Rev. Lett.* **118**, 087203 (2017).
54. Sibille, R. et al. Coulomb spin liquid in anion-disordered pyrochlore Tb₂Hf₂O₇. *Nat. Commun.* **8**, 892 (2017).
55. Sherman, N. E., Dupont, M. & Moore, J. E. Spectral function of the J_1 - J_2 Heisenberg model on the triangular lattice. *Phys. Rev. B* **107**, 165146 (2023).

Publisher's note Springer Nature remains neutral with regard to jurisdictional claims in published maps and institutional affiliations.

Springer Nature or its licensor (e.g. a society or other partner) holds exclusive rights to this article under a publishing agreement with the author(s) or other rightsholder(s); author self-archiving of the accepted manuscript version of this article is solely governed by the terms of such publishing agreement and applicable law.

© The Author(s), under exclusive licence to Springer Nature Limited 2024

Methods

Neutron scattering measurements

Single crystals of $\text{YCu}_3(\text{OD}_5\text{Br}_2[\text{Br}_{0.33}(\text{OD})_{0.67}])$ were grown using the hydrothermal method reported previously³⁸. About 5,000 single crystals were co-aligned on two Cu plates under an optical microscope with the CYTOP glue for the INS measurements, which were carried out on a cold-neutron disk chopper spectrometer AMATERAS at J-PARC (ref. 56). All the spectral data gathered by AMATERAS were processed with the software suite Utsusemi⁵⁷. The crystal assembly was aligned in the $[H, 0, L]$ scattering plane and mounted on a ^3He insert installed in a standard cryostat. The elastic neutron scattering results were obtained on the CAMEA multiplexing neutron spectrometer at the Paul Scherrer Institute, Switzerland^{58,59}, where the crystal assembly was aligned in the $[H, K, 0]$ scattering plane and measured in a dilution refrigerator. The momentum transfer Q in three-dimensional reciprocal space is defined as $Q = H\mathbf{a}^* + K\mathbf{b}^* + L\mathbf{c}^*$, where H, K and L are Miller indices and $\mathbf{a}^* = 2\pi(\mathbf{b} \times \mathbf{c})/V$, $\mathbf{b}^* = 2\pi(\mathbf{c} \times \mathbf{a})/V$ and $\mathbf{c}^* = 2\pi(\mathbf{a} \times \mathbf{b})/V$, with $a = b = 6.6779 \text{ \AA}$, $c = 5.9874 \text{ \AA}$ and $V = 231.23 \text{ \AA}^3$ for the kagome lattice.

Theoretical calculations

We calculated the spectrum of a linear spin wave using the Heisenberg model of a kagome lattice with three different couplings, which form the effective Hamiltonian of $\text{YCu}_3\text{-Br}$. Linear spin wave theory describes the dynamics of spins around their classical direction under small quantum fluctuations. Here, the term ‘small’ refers to a quantum fluctuation that can be explained by expanding the Hamiltonian as a function of S using the Holstein–Primakoff approximation⁶⁰. Our results show that the INS results presented in the text are beyond the small perturbation of the magnetically ordered ground state, such as the classical $(1/3, 1/3)$ order considered here. Our calculations were made with the SPINW package⁴⁸ and their details are presented in the Supplementary Information (in which we include more information on the INS experiment and the calculation of the linear spin wave analysis for Heisenberg model on kagome lattice).

Data availability

All relevant data supporting the findings of this study are available from the corresponding authors on reasonable request. Source data are provided with this paper.

References

- Nakajima, K. et al. AMATERAS: a cold-neutron disk chopper spectrometer. *J. Phys. Soc. Jpn* **80**, SBO28 (2011).
- Inamura, Y., Nakatani, T., Suzuki, J. & Otomo, T. Development status of software ‘Utsusemi’ for chopper spectrometers at MLF, J-PARC. *J. Phys. Soc. Jpn* **82**, SA031 (2013).
- Lass, J., Jacobsen, H., Mazzone, D. G. & Lefmann, K. MJOLNIR: a software package for multiplexing neutron spectrometers. *SoftwareX* **12**, 100600 (2020).

- Lass, J. et al. Commissioning of the novel continuous angle multi-energy analysis spectrometer at the Paul Scherrer Institut. *Rev. Sci. Instrum.* **94**, 023302 (2023).
- Holstein, T. & Primakoff, H. Field dependence of the intrinsic domain magnetization of a ferromagnet. *Phys. Rev.* **58**, 1098–1113 (1940).

Acknowledgements

We thank Y. Zhou, Y. Li and P. Lee for discussions. This work is supported by the National Key Research and Development Program of China (Grant Nos. 2022YFA1403400 and 2021YFA1400401), the K. C. Wong Education Foundation (Grant No. GJTD-2020-01), the Strategic Priority Research Program (B) of the Chinese Academy of Sciences (Grant No. XDB33000000) and the Research Grants Council of Hong Kong Special Administrative Region of China (Project Nos. 17301721, AoE/P701/20, 17309822, C7037-22GF, A_HKU703/22 and 17302223). Measurements on AMATERAS were performed based on the approved proposal (Grant No. 2022B0048). The measurement on CAMEA was carried out under the proposal number 20220991. We thank HPC2021 system under the Information Technology Services and the Blackbody HPC system at the Department of Physics, University of Hong Kong, as well as the Beijing PARATERA Tech CO., Ltd. (<https://cloud.paratera.com>).

Author contributions

Z.Z. grew the samples and analysed the INS data. C.Z., R.C. and Z.Y.M. performed the theoretical analysis and calculations. H.Z. and L.H. helped in co-aligning the crystals. K.L. helped in preparing the deuterated samples. M.K., K.N., Y.W., W.Z. and D.G.M. carried out the neutron scattering experiments. Z.Y.M. and S.L. drafted the paper with input from all authors. S.L. designed and supervised the project.

Competing interests

The authors declare no competing interests.

Additional information

Supplementary information The online version contains supplementary material available at <https://doi.org/10.1038/s41567-024-02495-z>.

Correspondence and requests for materials should be addressed to Kenji Nakajima, Zi Yang Meng or Shiliang Li.

Peer review information *Nature Physics* thanks the anonymous reviewer(s) for their contribution to the peer review of this work.

Reprints and permissions information is available at www.nature.com/reprints.